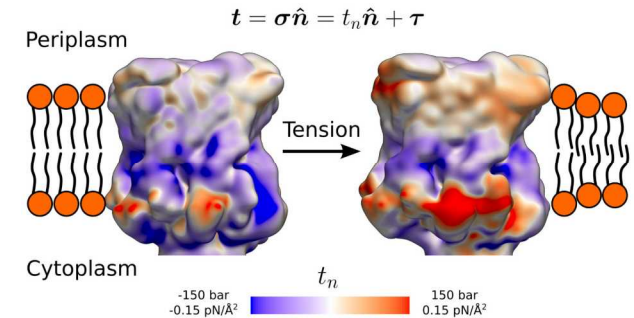
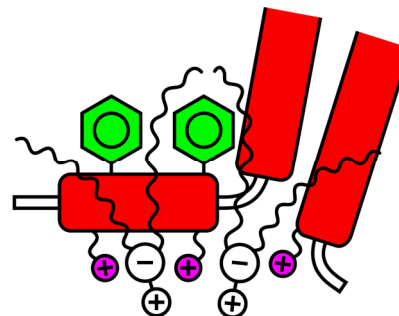
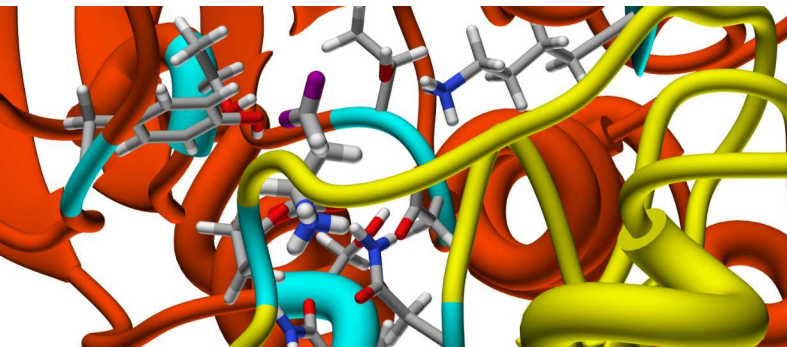


Exceptional service in the national interest



Computational “microscopy”: Probing sub-cellular function with molecular modeling

Juan Vanegas

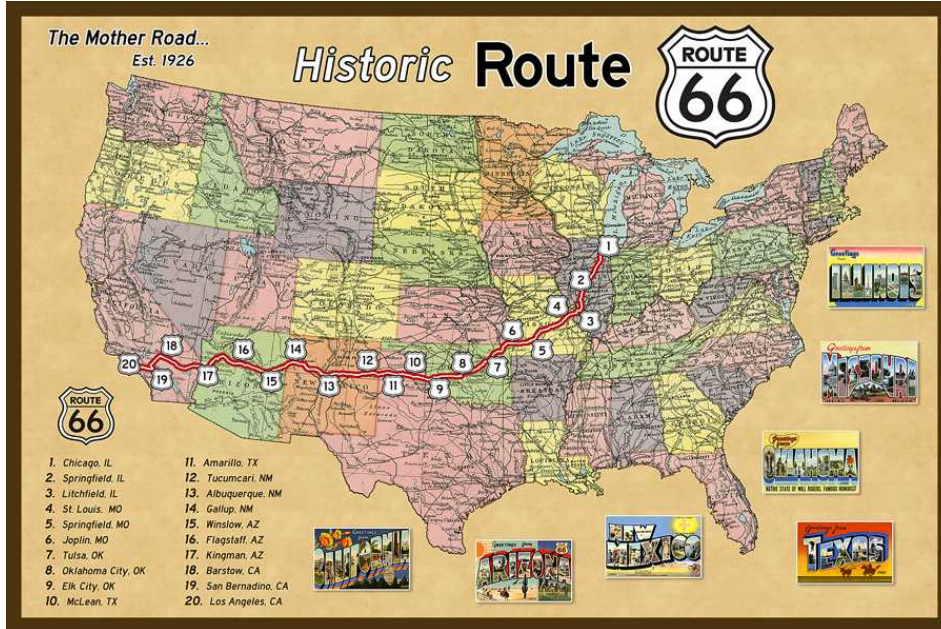
Nanobiology Department

Center for Biological and Material Sciences

Sandia National Laboratories



Sandia National Laboratories is a multi-program laboratory managed and operated by Sandia Corporation, a wholly owned subsidiary of Lockheed Martin Corporation, for the U.S. Department of Energy's National Nuclear Security Administration under contract DE-AC04-94AL85000. SAND NO. 2015-



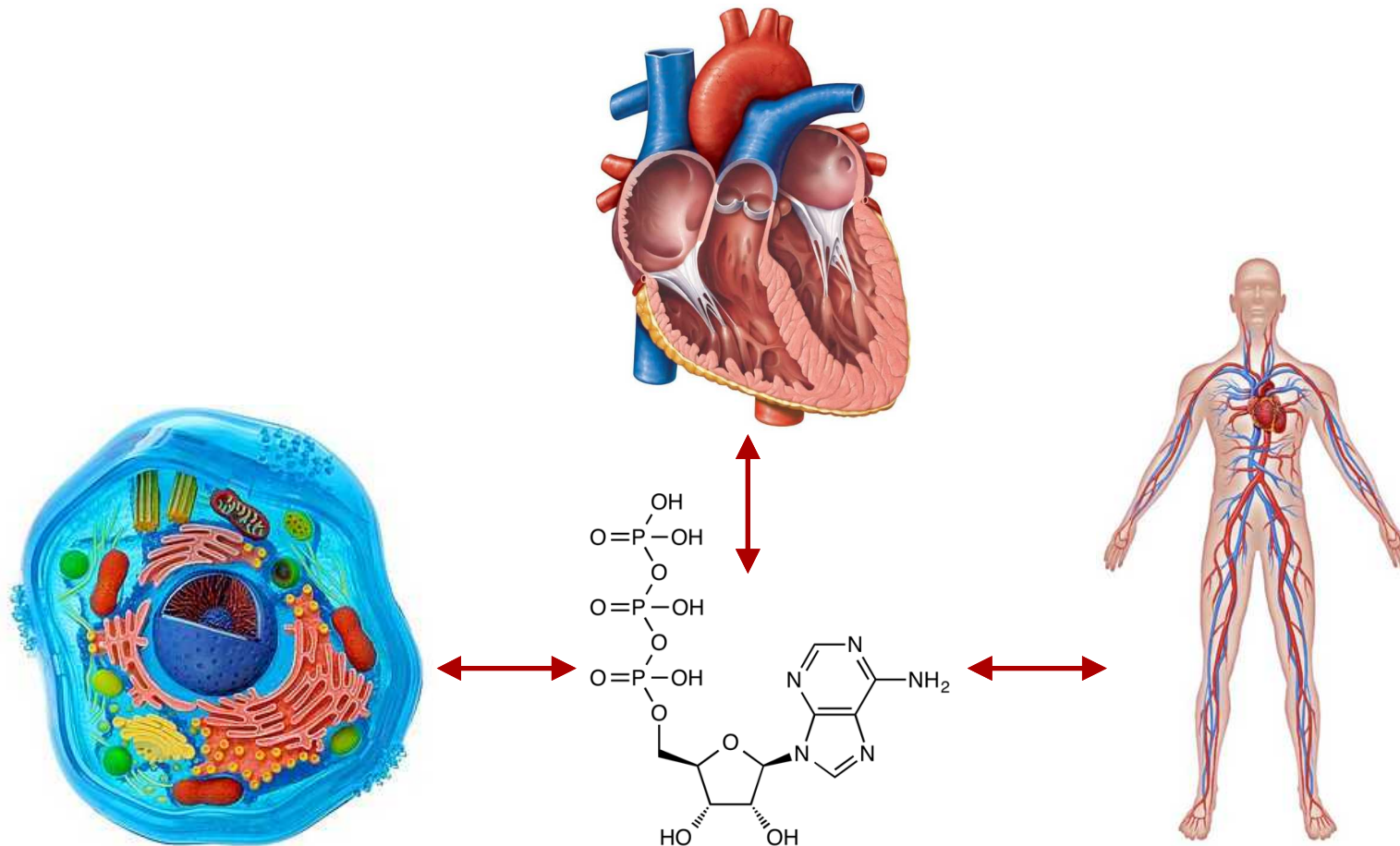
Sandia - New Mexico



Sandia - California

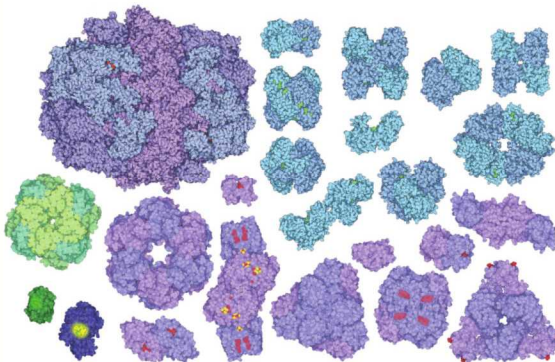
From molecules to organisms

- Biological function across the scales is intimately connected to the interaction of atoms and molecules at the nm level

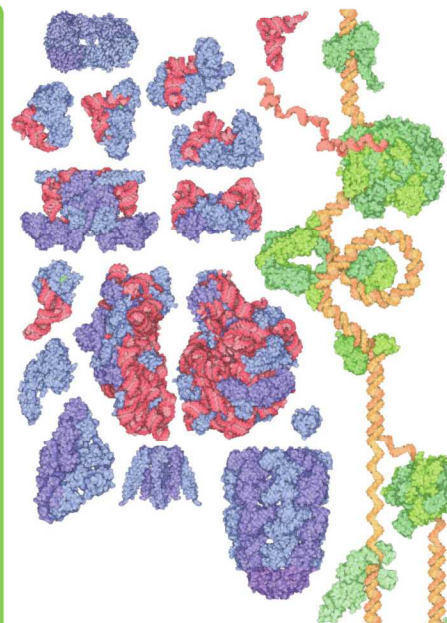


Molecular machines

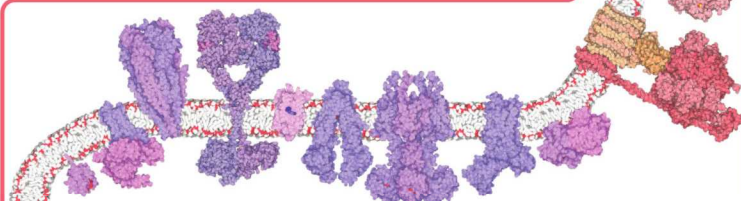
Enzymes



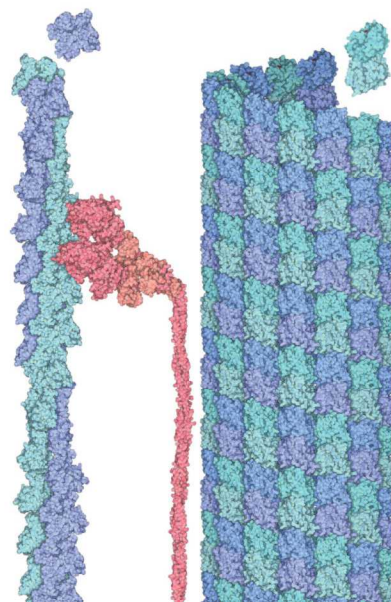
Protein synthesis - nucleic acid processing



Lipid membrane - membrane proteins



Cytoskeletal - Structural proteins



Images from rcsb.org

Computational “microscopy”

- How can we probe structure-function relationships in molecular systems with computational models?
- Molecular dynamics (MD) simulations
 - Classical trajectories of interacting point particles

$$\mathbf{F}_i = m_i \ddot{\mathbf{r}}_i = -\nabla_{\mathbf{r}_i} V(\mathbf{r}_1, \dots, \mathbf{r}_N)$$

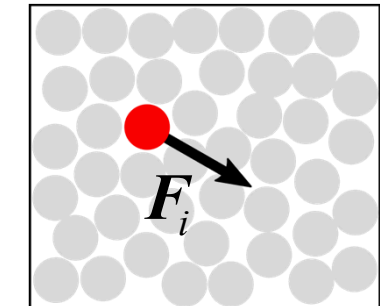
$$\mathbf{r}_i(t + \Delta t) = 2\mathbf{r}(t) - \mathbf{r}(t - \Delta t) + \ddot{\mathbf{r}}(t)\Delta t^2 + O(\Delta t^4)$$

- Interaction potentials

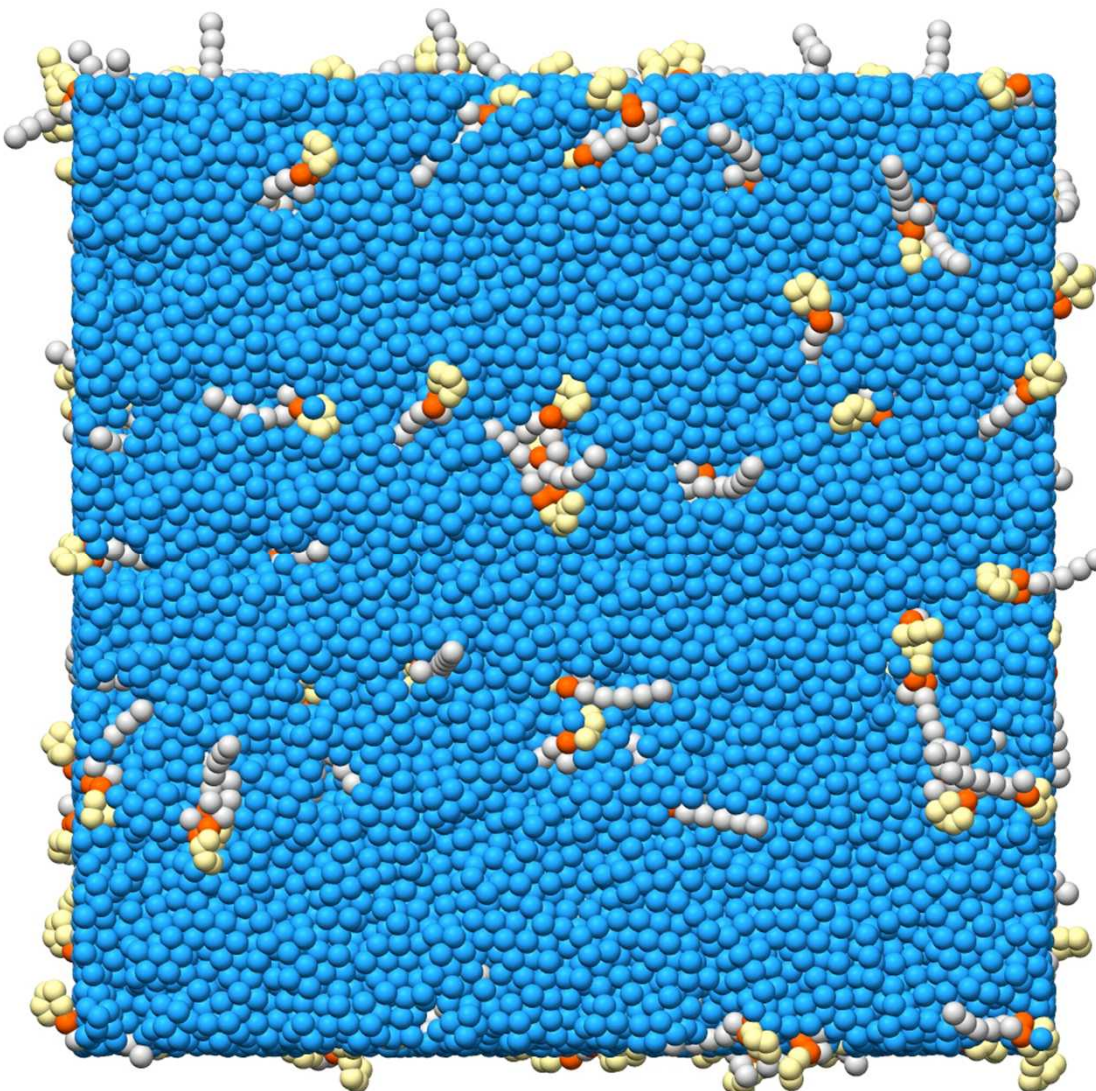
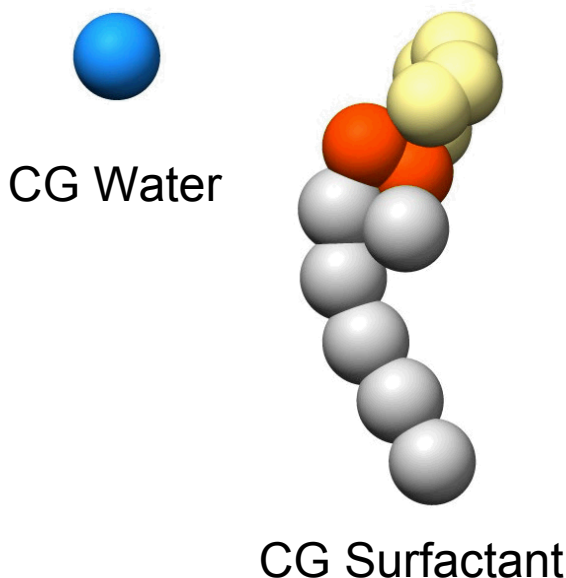
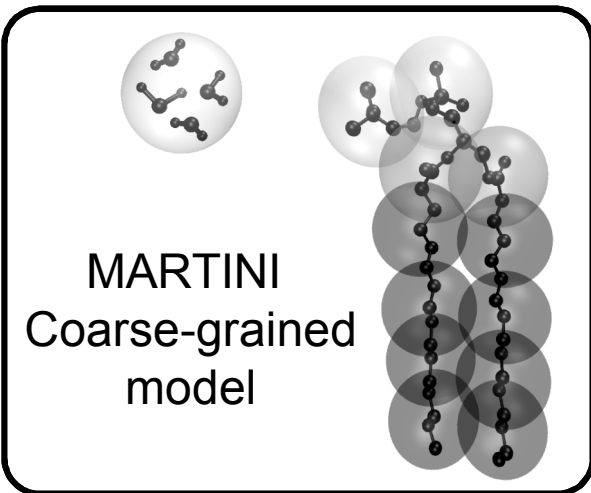
$$V(\mathbf{r}_1, \dots, \mathbf{r}_N) = V_{\text{VdW}} + V_{\text{Coul}} + V_{\text{bonds}} + V_{\text{angles}} + V_{\text{torsions}} + \dots$$

$$\sum_{i=1}^N \sum_{j=i+1}^N \left(4\epsilon_{ij} \left[\left(\frac{\sigma_{ij}}{r_{ij}} \right)^{12} - \left(\frac{\sigma_{ij}}{r_{ij}} \right)^6 \right] + \frac{q_i q_j}{4\pi\epsilon_0 r_{ij}} \right)$$

angles $\sum_{\text{angles}} \frac{u_i}{2} (\theta_i - \theta_{i,0})^2$
 bonds $\sum_{\text{bonds}} \frac{k_i}{2} (l_i - l_{i,0})^2$



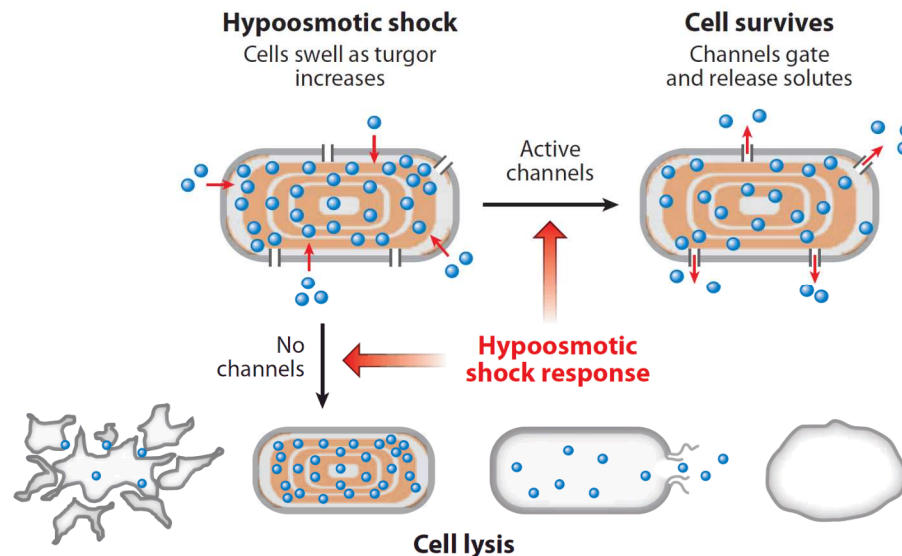
MD in action: Surfactant self-assembly



Mechanical signal transduction in the bacterial MscL channel

Mechanosensation in biology

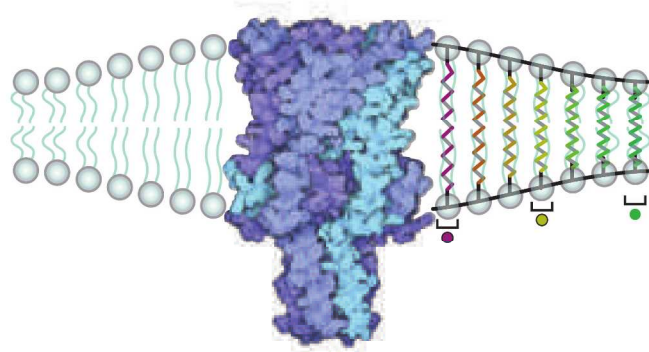
- Conversion of external/mechanical stimuli into electrochemical signals
 - Sensing touch, hearing (vibrations), movement (balance)
 - Sensing gravity (gravitropism)
 - Sensing changes in cell volume/shape (growth and development)
 - Vascular pressure control
 - Osmotic regulation



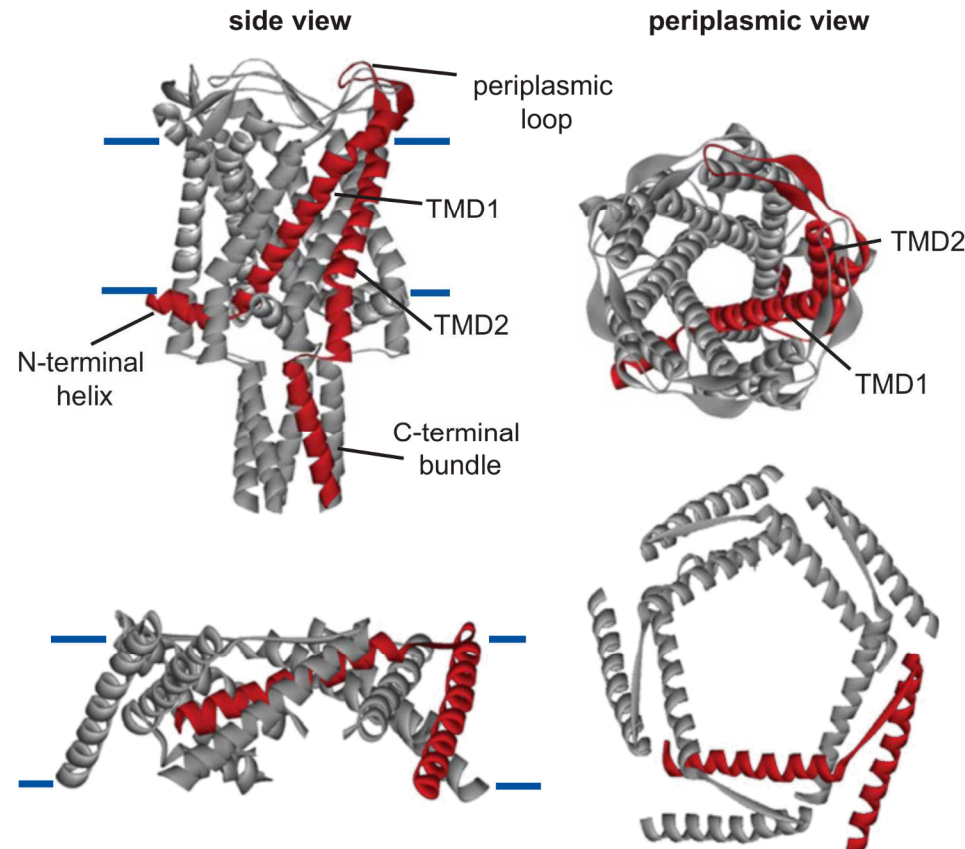
Naismith & Booth. *Annu. Rev. Biophys.* 41, 157–77 (2012)

Bacterial MscL channel

- Mechanosensitive channel of large conductance
 - Unselective channel with large opening – cell's last resort before lysis



Phillips et al. *Nature*. 459, 379-385 (2009)

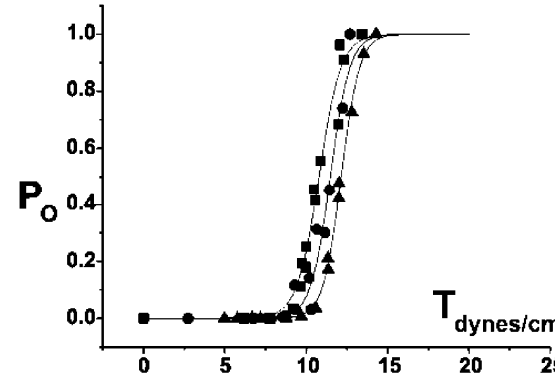
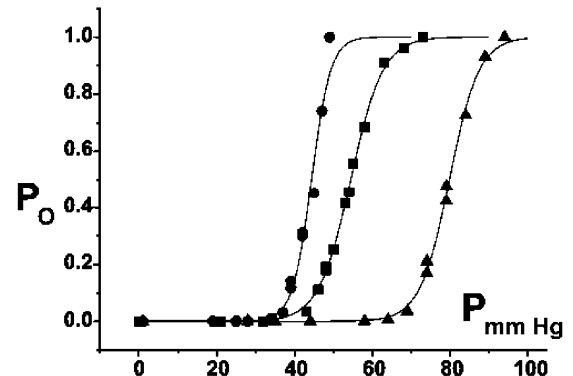


Iscla & Blount. *Biophys. J.* 103, 169-174 (2012)

9

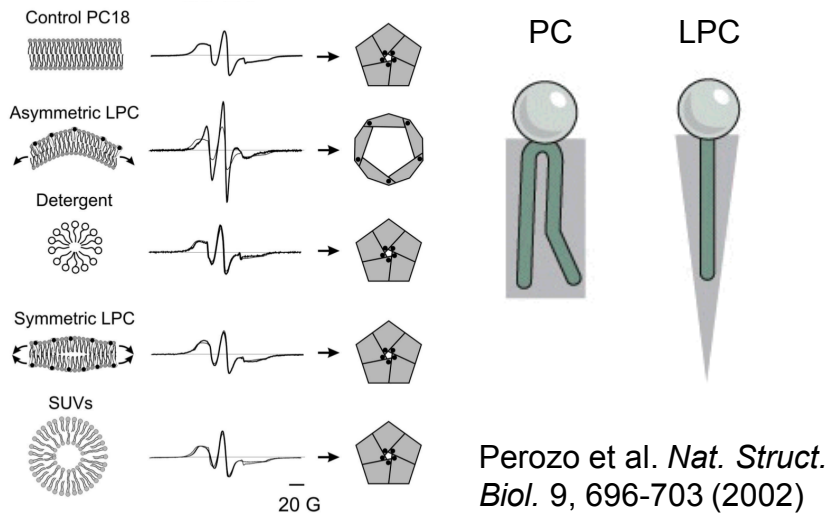
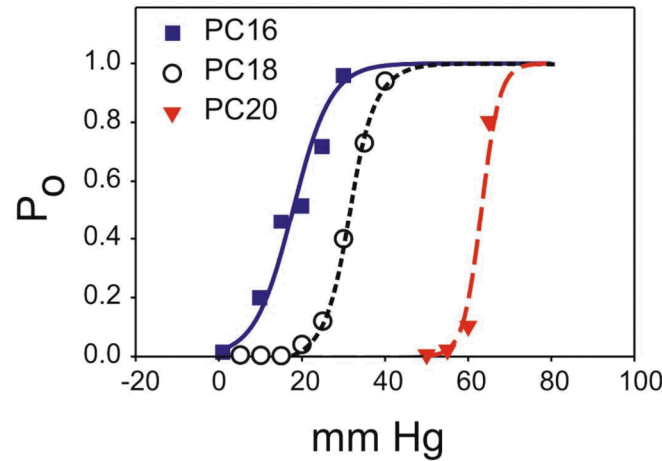
What actuates the channel?

- Channel senses tension in the membrane, not pressure differences



Moe & Blount. *Biochemistry*.
44, 12239-12244 (2005)

- Gating is sensitive to bilayer thickness and conical (lyso) lipids

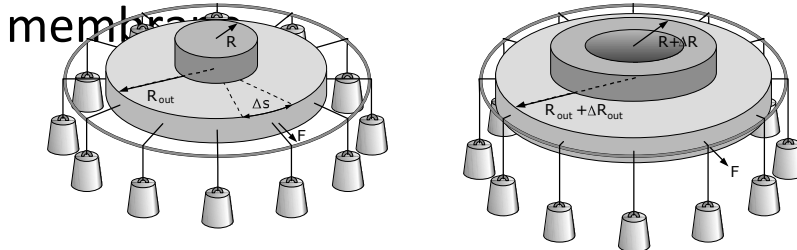


Perozo et al. *Nat. Struct. Biol.* 9, 696-703 (2002)

Local stress, elasticity and gating

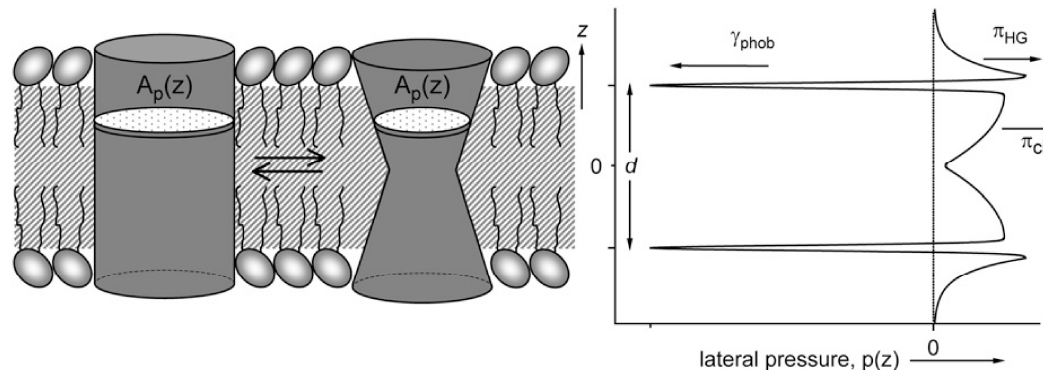
- Gating energetics can be estimated by various models

- Continuum models that characterize elastic deformation of membranes



Wiggins & Phillips. *Biophys. J.* 88, 880-902 (2005)
 Phillips et al. *Nature*. 459, 379-385 (2009)
 Reeves et al. *Phys. Rev. E* 78, 041901 (2008)

- Internal stress or “lateral pressure” in the membrane may modulate



Marsh. *Biophys. J.* 93, 3884-3899 (2007)

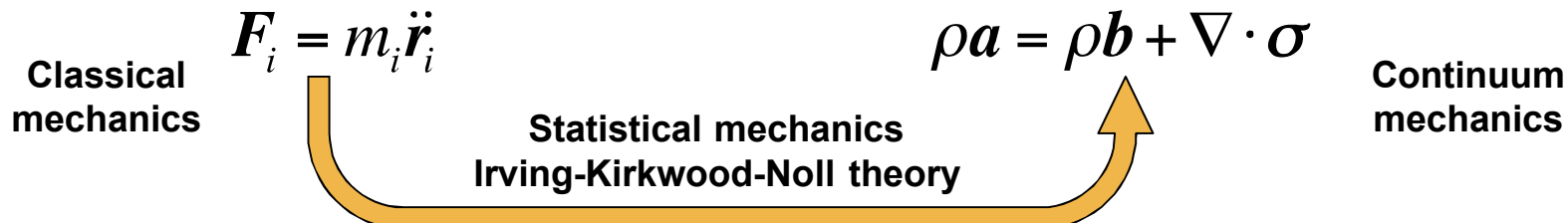
- Changes in area due to pressure/surface tension

$$W = \int P(z) \Delta A(z) dz$$

Marshall. *Biophys. J.* 100, 1651-1659 (2011)
 Gullingsrud & Schulten. *Biophys. J.* 86, 3496-3509 (2004)

Bridging continuum & molecular models

- Continuum fields can be obtained from particle-based MD simulations through ensemble averaging



The diagram illustrates the connection between three fields: Classical mechanics, Statistical mechanics, and Continuum mechanics. It features three equations arranged horizontally. On the left, under 'Classical mechanics', is the equation $F_i = m_i \ddot{r}_i$. In the center, under 'Statistical mechanics' (Irving-Kirkwood-Noll theory), is the equation $\rho a = \rho b + \nabla \cdot \sigma$. On the right, under 'Continuum mechanics', is the equation $\nabla \cdot \sigma = \nabla \cdot \left(\sum_{i=1}^N \langle m_i \mathbf{v}_i \otimes \mathbf{v}_i \delta(\mathbf{r}_i - \mathbf{x}) \rangle \right) - \sum_{i=1}^N \langle F_i \delta(\mathbf{r}_i - \mathbf{x}) \rangle$. A thick orange curved arrow connects the first two equations to the third, indicating that the Irving-Kirkwood-Noll theory provides the link between the microscopic dynamics of particles and the macroscopic continuum mechanics stress tensor.

$$F_i = m_i \ddot{r}_i$$
$$\rho a = \rho b + \nabla \cdot \sigma$$
$$\nabla \cdot \sigma = \nabla \cdot \left(\sum_{i=1}^N \langle m_i \mathbf{v}_i \otimes \mathbf{v}_i \delta(\mathbf{r}_i - \mathbf{x}) \rangle \right) - \sum_{i=1}^N \langle F_i \delta(\mathbf{r}_i - \mathbf{x}) \rangle$$

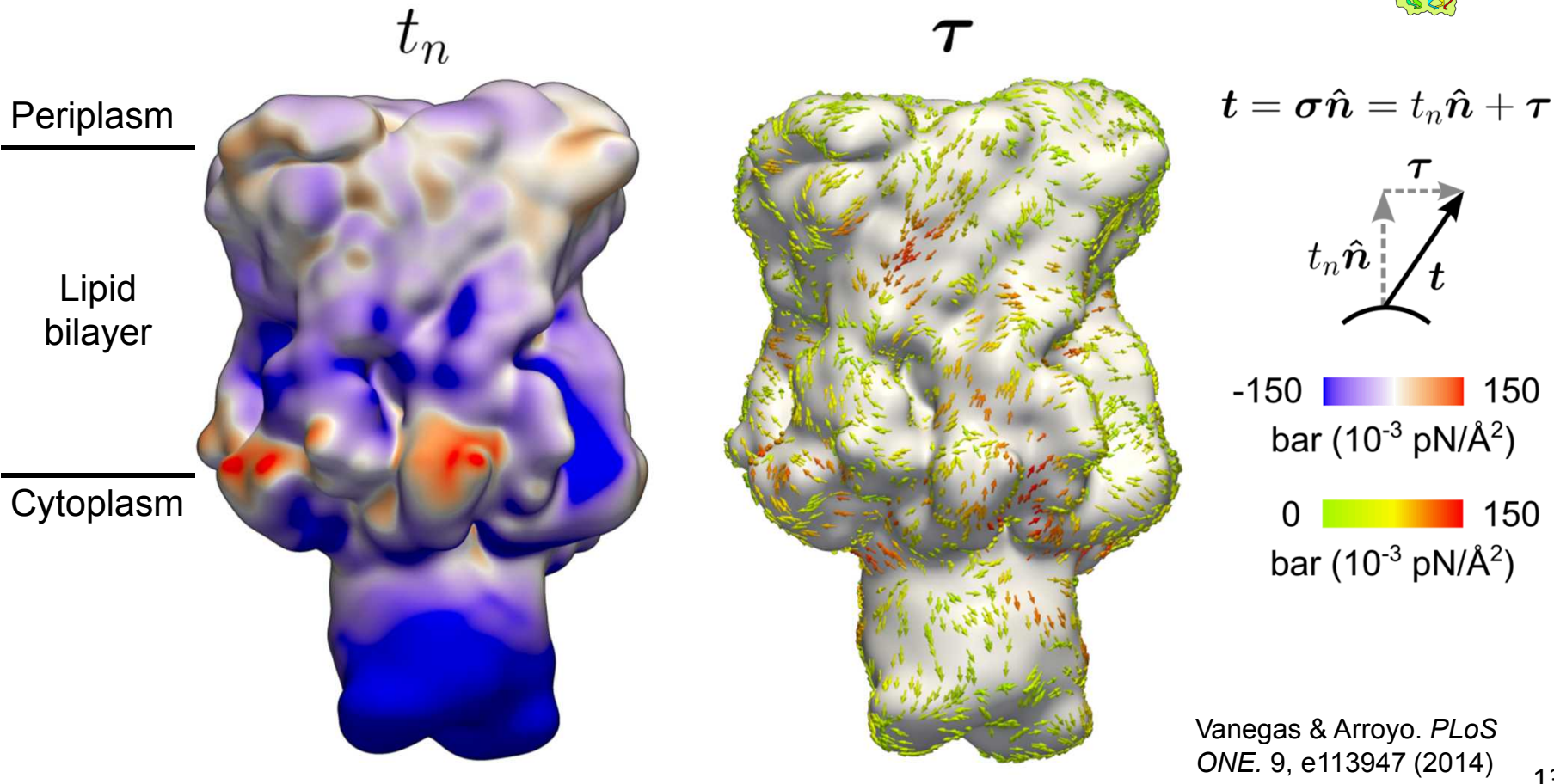
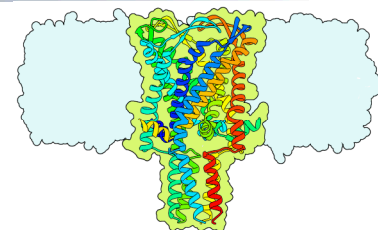
- Microscopic stress field (3D) from MD simulations (time avg)

$$\sigma = \frac{1}{N_\tau} \sum_t^{N_\tau} \left[- \sum_i^N m_i \mathbf{v}_{i(t)} \otimes \mathbf{v}_{i(t)} w(\mathbf{r}_{i(t)} - \mathbf{x}) + \frac{1}{2} \sum_{\substack{i,j \\ i \neq j}}^N \mathbf{f}_{ij(t)} \otimes \mathbf{r}_{ij(t)} B(\mathbf{x}; \mathbf{r}_{i(t)}, \mathbf{r}_{j(t)}) \right]$$

Vanegas, Torres-Sanchez, & Arroyo. *J. Chem. Theory Comput.* 10, 691-702 (2014)
Torres-Sanchez, Vanegas, & Arroyo. *Phys. Rev. Lett.* 114, 258102 (2015)

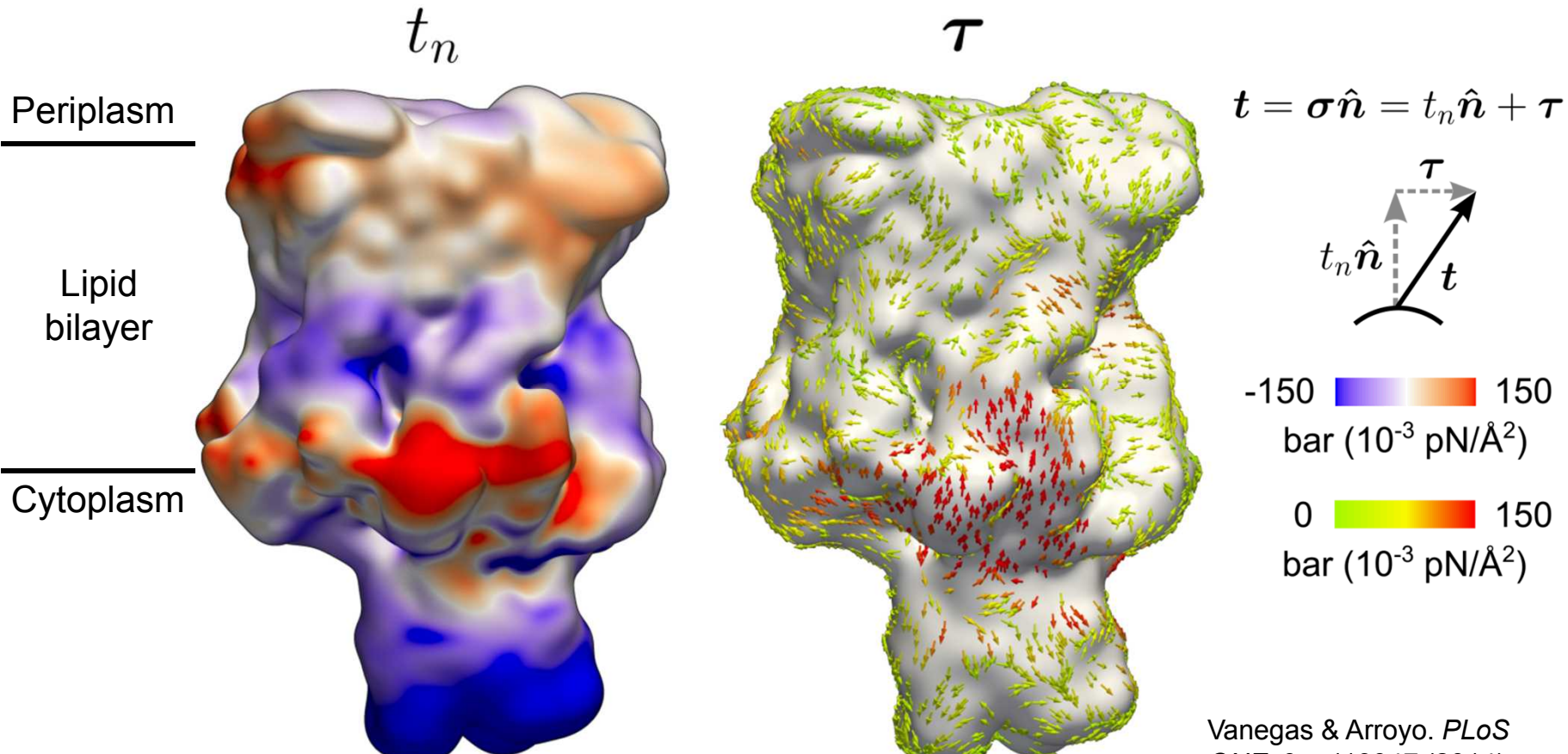
Local stress on the surface of MscL

- MscL simulated in a membrane patch (~500 lipids)
- 3D stress visualized as traction vector on surface



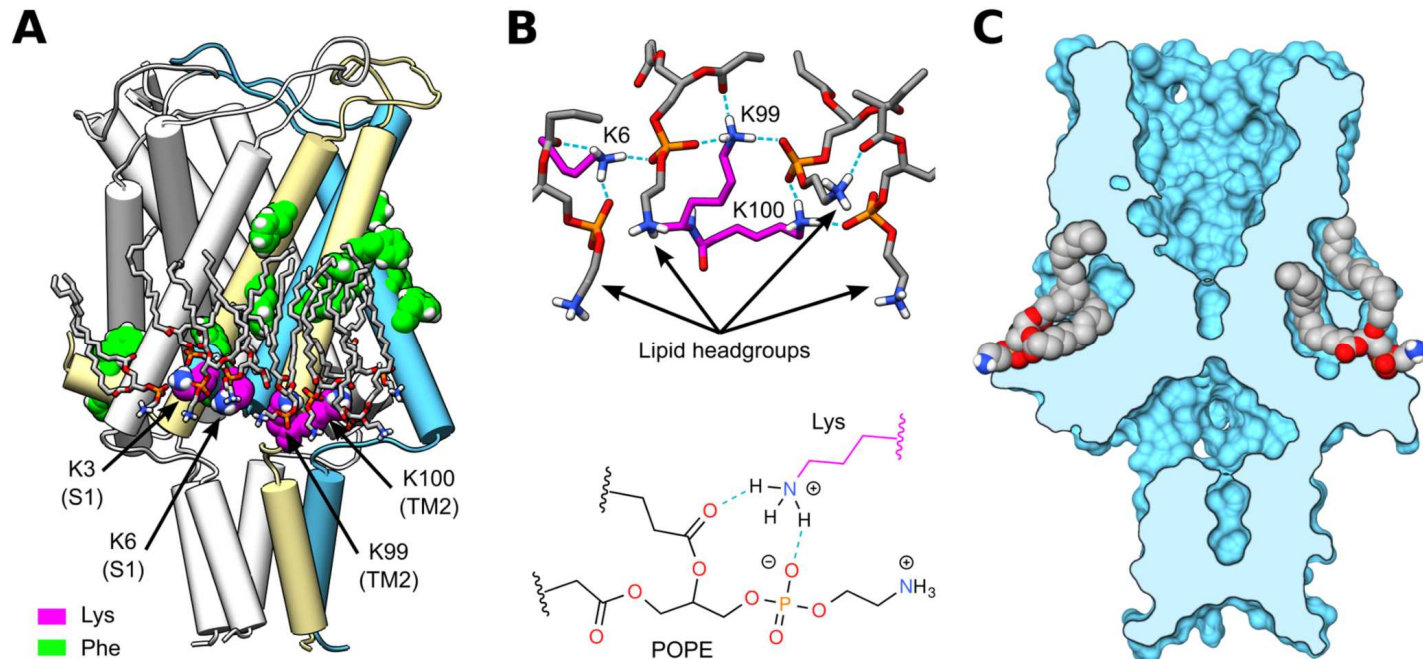
Stress “hot-spots” under tension

- Membrane under tension ($P_L = -20$ bar, $\sim 6\%$ lateral stretch)
- Channel remains in closed quasi-equilibrium state



Lipid binding on the cytoplasmic side

- Two lipids associate with each MscL monomer at specific sites
 - Locations match stress hot-spots**
 - + Charged lysines on C-terminus and TM2 (K3, K6, K99, K100) interact with electronegative oxygens on the POPE lipid headgroup
 - Lipid tails accommodate in hydrophobic cavities – preference for 16 vs 18 carbon tail (8 out of 10) of POPE



Energetics of lipid unbinding

- What is the interaction energy between bound lipids and MscL?

- Lipid unbinding kinetics under a pulling force

$$d\phi/dt = (1 - \phi) k_d \Rightarrow \phi(t) = 1 - e^{-k_d t}$$

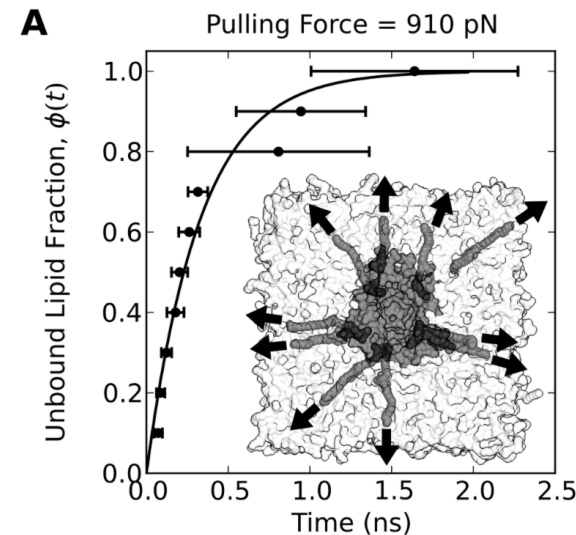
- Simple Arrhenius-Bell model (assuming electrostatic interaction dominates)

$$E_b(f) = E_0 - f x_b$$

$$k_d(f) = 1/t_d e^{-(E_0 - f x_b)/k_B T}$$

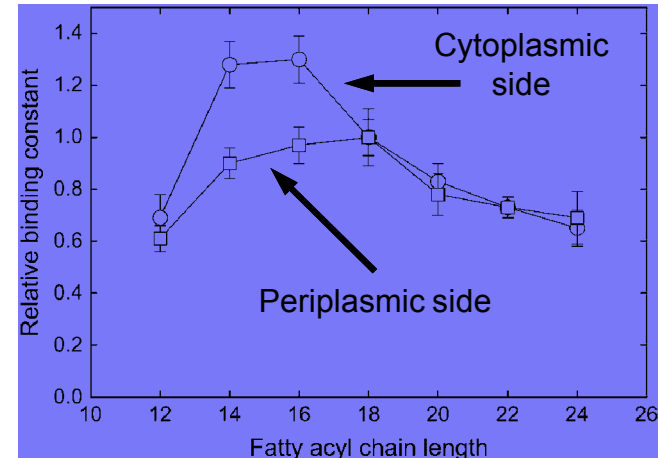
$$k_d(f) = 1/t_{off} e^{f x_b/k_B T}$$

- Energy barrier in range of 10-13 $k_B T$

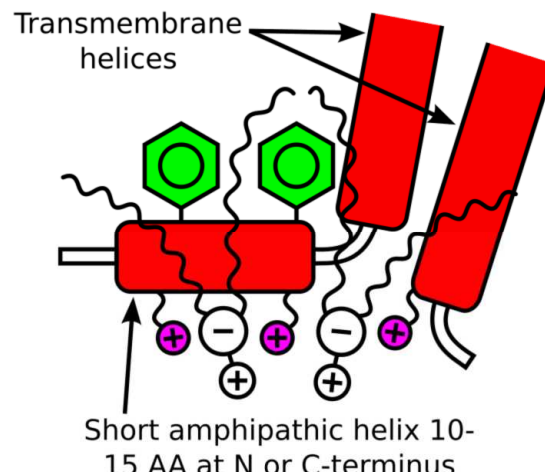


A resilient association

- Association of lipids with MscL observed experimentally
 - Higher affinity for cytoplasmic side and 16 carbon tails
- Lipid binding to MscL is simple and robust
 - Charged interactions + geometric confinement (lipid tail)



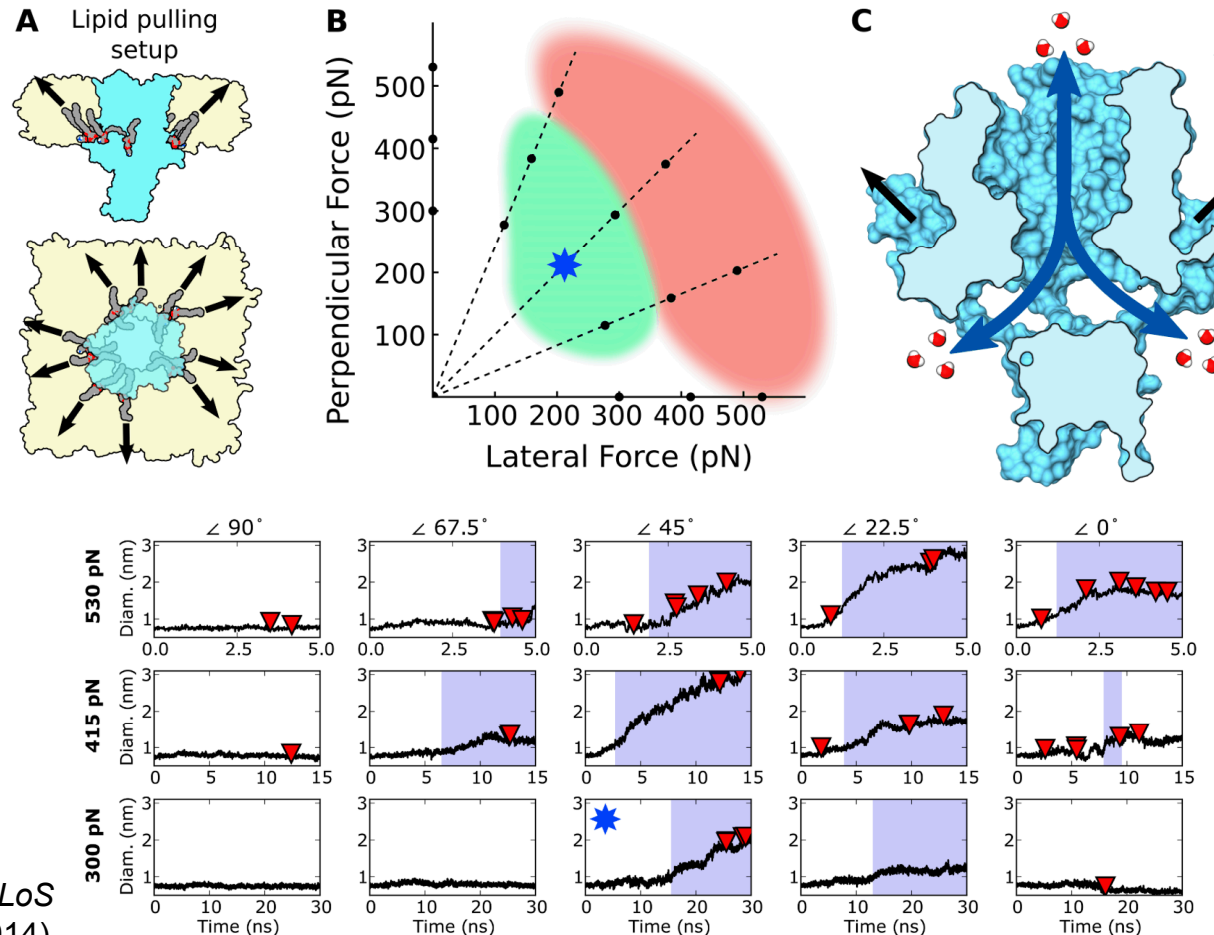
Powl et al. *Biophys. J.* 93, 113-122 (2007)



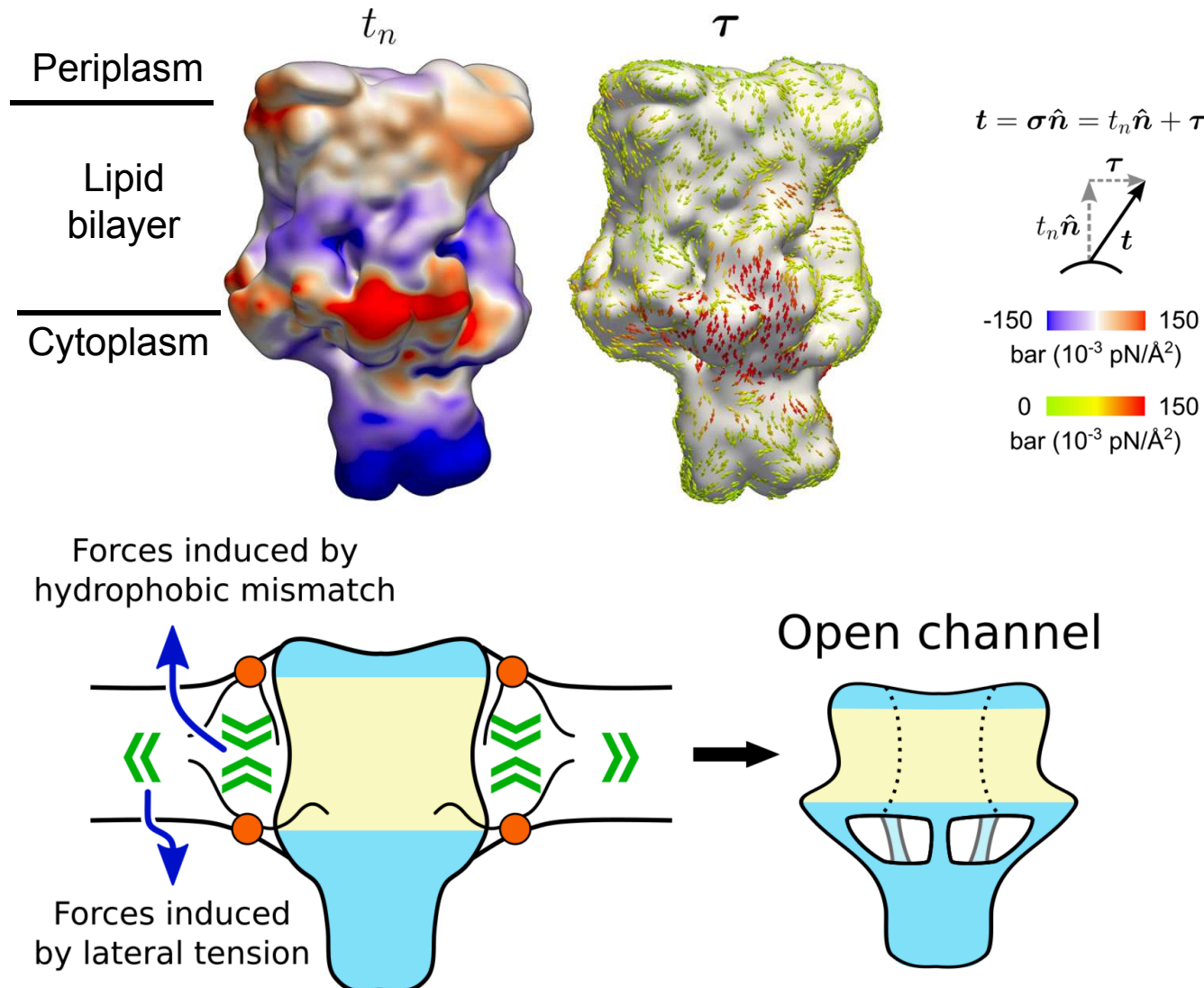
Vanegas & Arroyo.
PLoS ONE. 9,
e113947 (2014)

Actuating the channel in steered MD

- MscL gating by membrane tension is slow (microseconds)
 - Can the channel be actuated by pulling on the tightly-bound lipids?

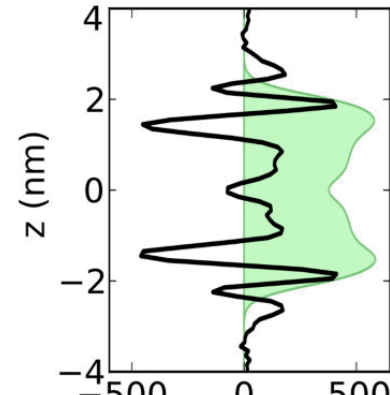
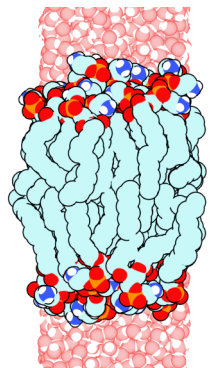


A framework for force transduction



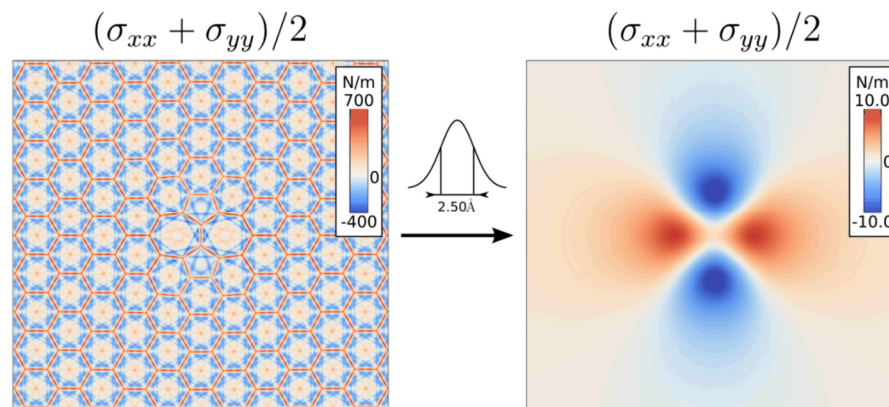
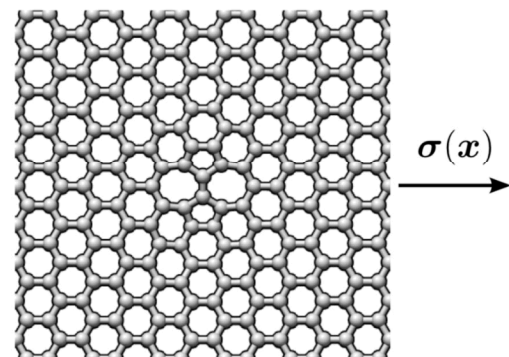
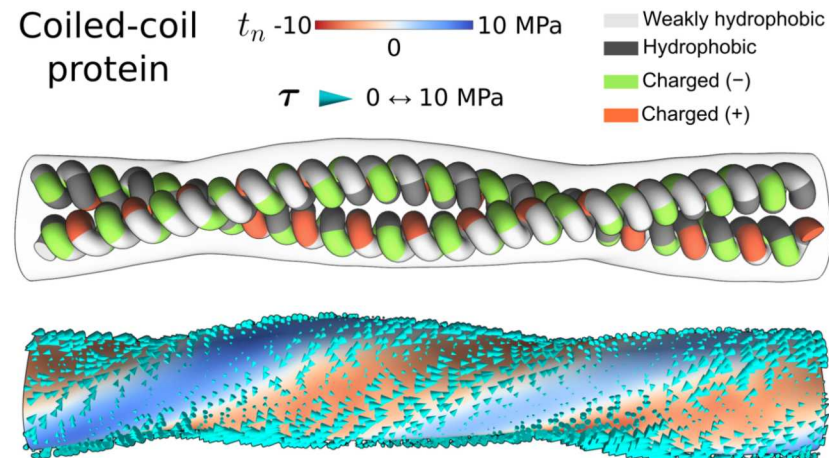
Other applications of local stress

- More info/code available at mdstress.org



Vanegas, Torres-Sanchez, &
Arroyo. *J. Chem. Theory
Comput.* 10, 691-702 (2014)

P_L (bar)

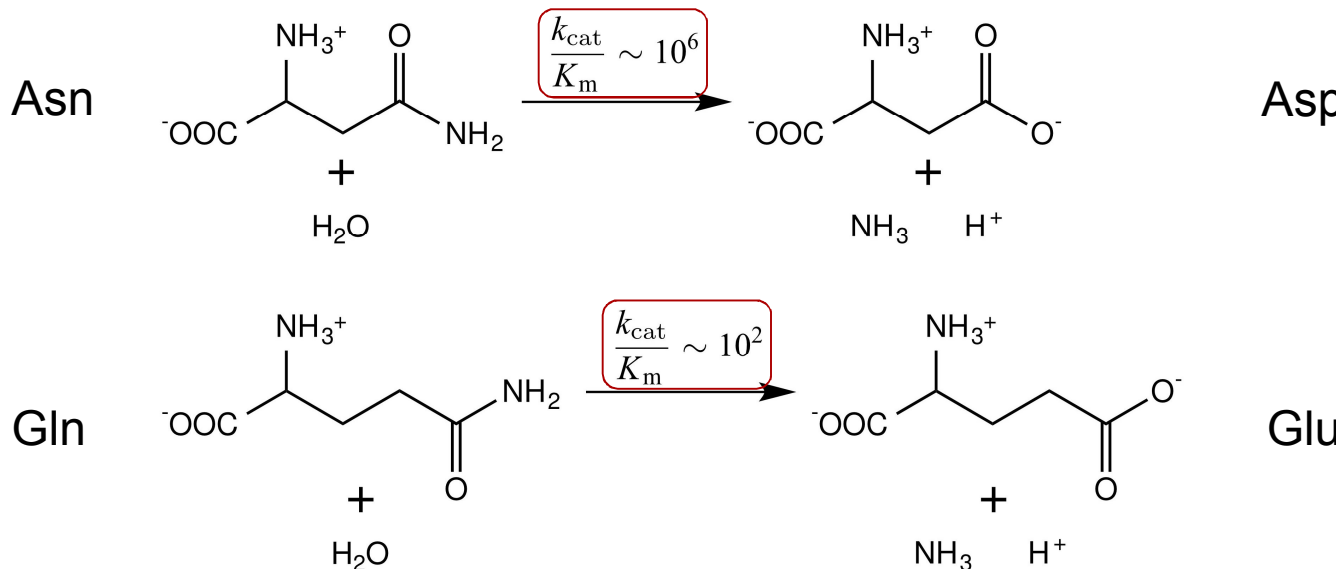


Torres-Sanchez, Vanegas, & Arroyo. *Phys. Rev. Lett.* 114, 258102 (2015)

Catalysis and specificity in L-Asparaginase, an anticancer enzyme

L-Asparaginase: Starving cancer cells

- Drug treatment against acute lymphoblastic leukemia
- L-ASP degrades amino acids Asn and Gln – starves certain cancer cells that can't synthesize these



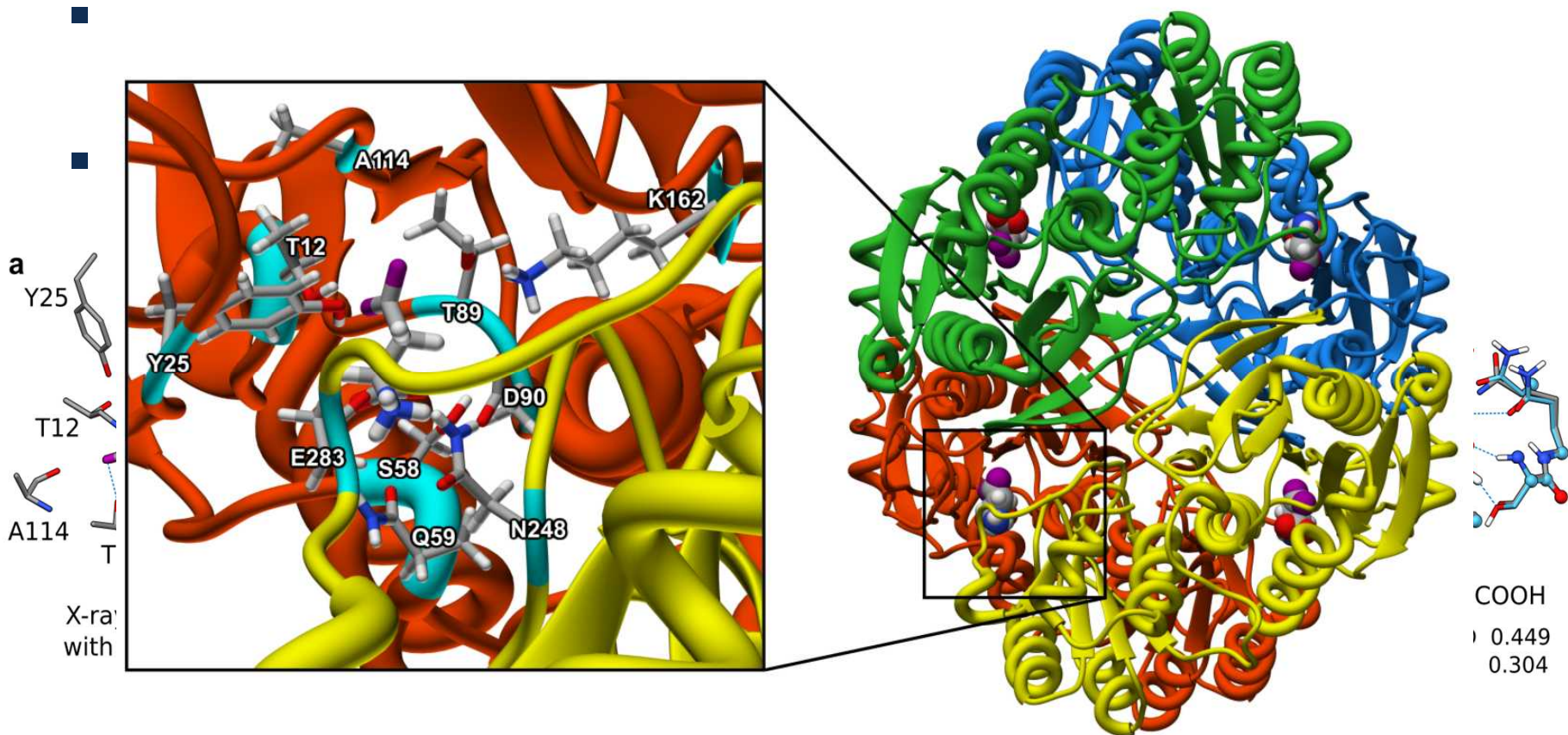
- L-ASP type II from *E. coli* (Elspar[®]) is most widely used clinically

Improving L-ASP's anticancer properties

- *E. coli* L-ASP has low catalytic rate – needs high doses for effective treatment (toxic side effects)
- Secondary glutaminase activity is also problematic
 - Linked to toxic side effects – precludes completion of treatment
 - Some cancers require degradation of both Asn and Gln
- How to optimize L-ASP for cancer treatment?
 - Tune substrate specificity – modulate glutaminase activity
 - Improve catalytic rate
- Despite 40+ years of clinical use, complete reaction mechanism remains unknown – limits rational engineering

Hidden proton in L-ASP's product

- Deamidation mechanisms rely heavily on crystal structure (PDB 1NNS) of L-ASP with the **reaction product Asp**

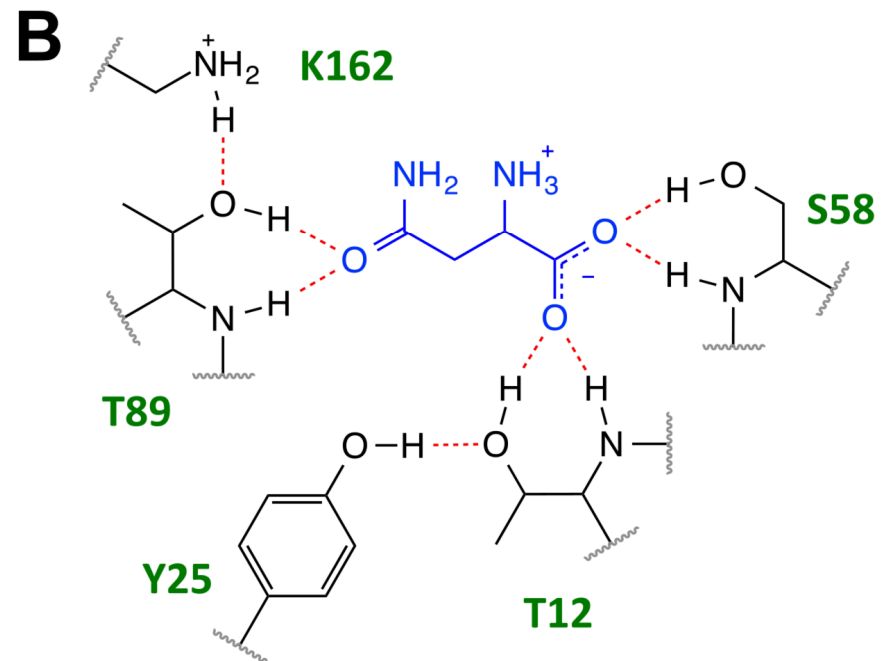
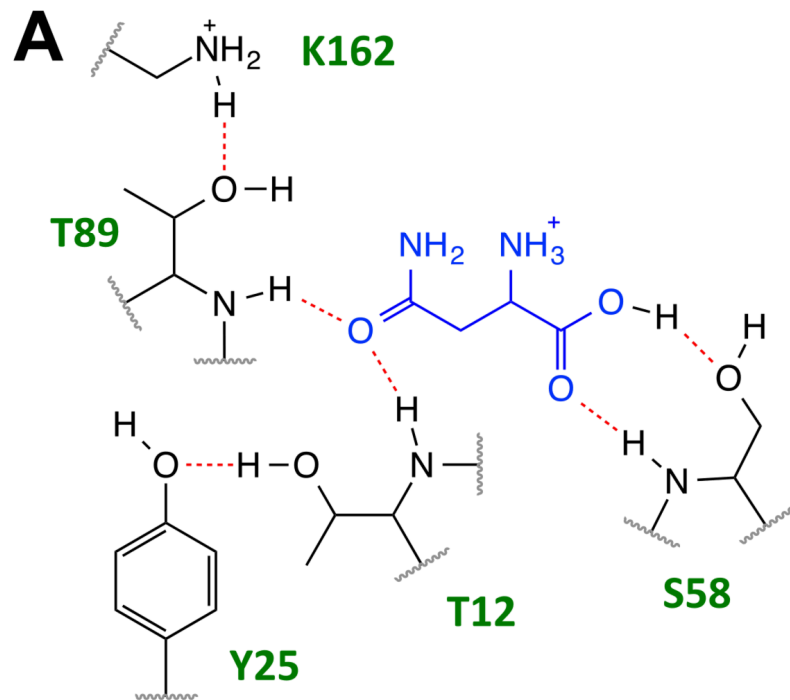


Anishkin, Vanegas et al. *J. Mol. Biol.* 427, 2867-2885 (2015)

24

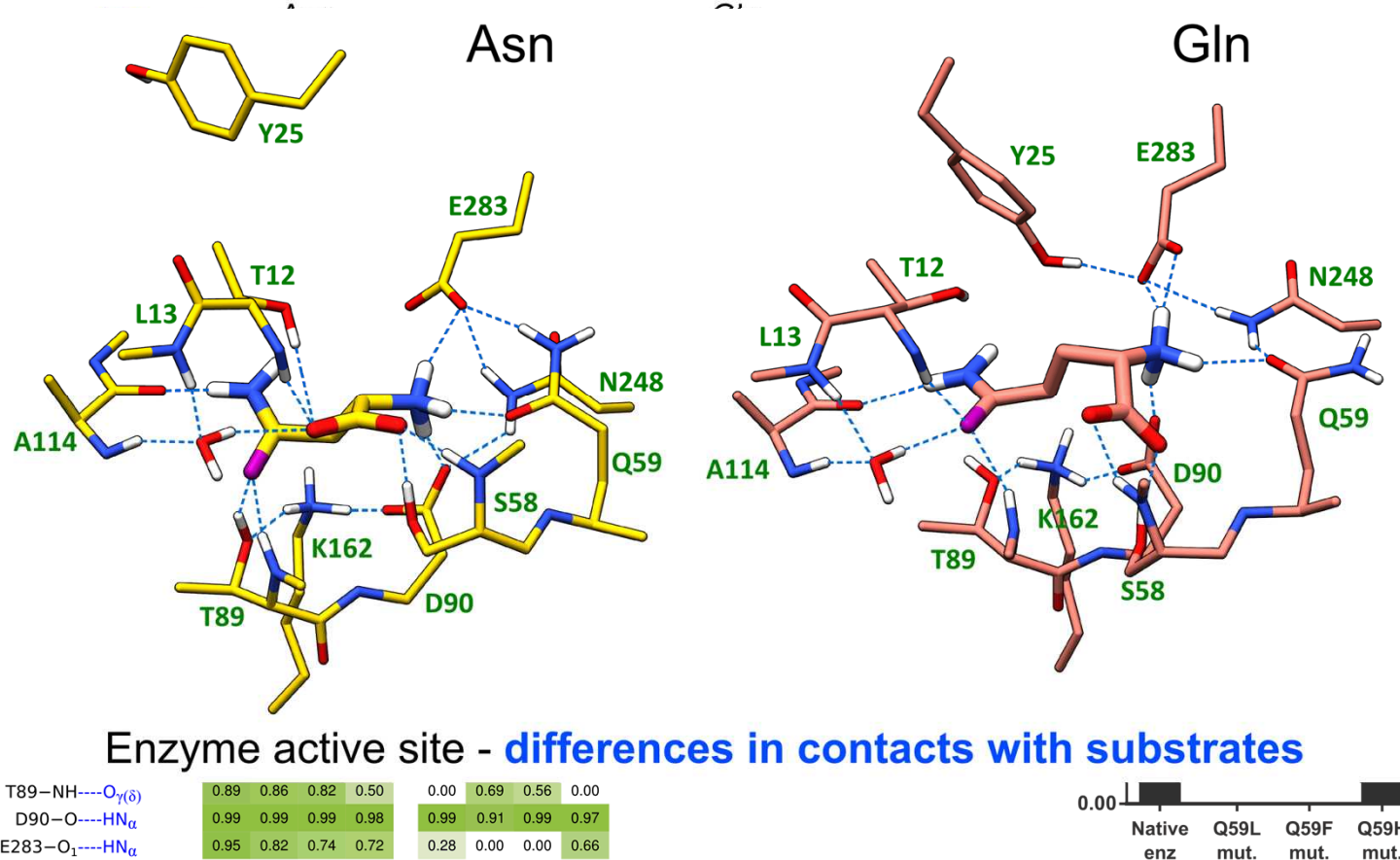
Substrate vs product conformations

- Asn substrate quickly rearranges in L-ASP active site
 - Unprotonated α -COO⁻ in Asn substrate induces large reorientation
 - T12, S58 and T89 “clamp” onto oxygens of Asn



Asn vs Gln: Tuning L-ASP's activity

- Can we alter L-ASP's active site to eliminate Gln degradation?
- Additional methylene in Gln affects substrate orientation



Chan et al. *Blood*. 123, 3596-5606 (2014); Anishkin, Vanegas et al. *J. Mol. Biol.* 427, 2867-2885 (2015)

L-ASP's mechanism puzzle

- Experiments strongly support double displacement mechanism with an acyl-enzyme covalent intermediate

kinetic experiments were performed with the asparagine analog β -hydroxamate (AHA) as the substrate. The activities of toward its natural substrate, L-asparagine, and AHA are compare. The latter substrate was preferred for the sensitive and reliable assay of its product, hydroxylamine (NH_2OH), with 8-hydroxy- N -phenanthroline [8].

initial burst' experiments, the time course of the appearance of

G.J. Palm et al./FEBS Letters 390 (1996) 21

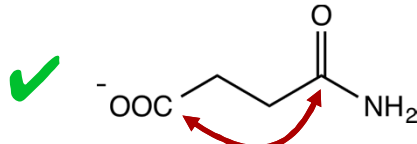
Palm et al. *FEBS Lett.*
390, 211-216 (1996)

lar size (determined by analytical gel filtration and SDS-acrylamide gel electrophoresis), and thermodynamical sties (derived from denaturation curves in guan hydrochloride solutions) were almost the same as those with wild-type EcA (data not shown).

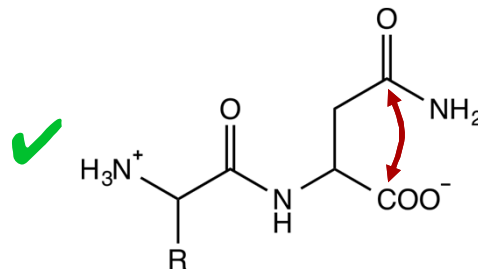
Despite the different crystal forms ($\text{P}2_1\text{2}_1\text{2}_1$ vs. $\text{P}2_1$

- L-ASP's threonine T12 and T89 are possible nucleophiles
 - T89V and T12A single mutants both reduce k_{cat} \sim 100,000 fold
- Absolute requirement of carboxyl group 2-3 carbons from amide

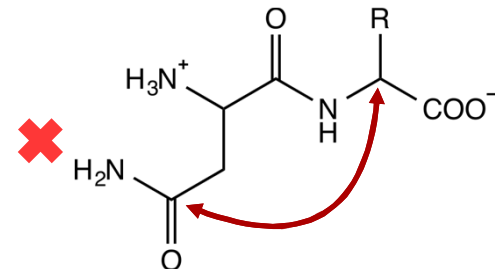
succinamate



$\text{NH}_3^+ \text{-Xxx-Asn-COO}^-$

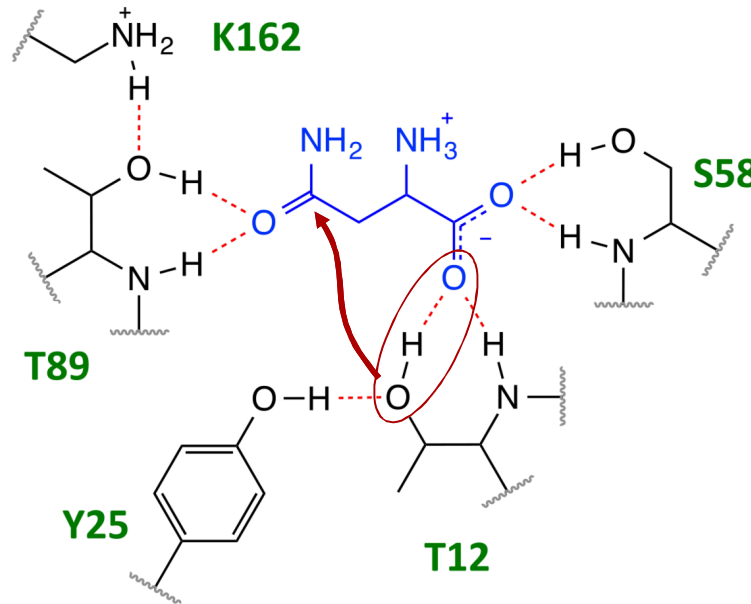


$\text{NH}_3^+ \text{-Asn-Xxx-COO}^-$



Initial stages of the reaction

- Focus on nucleophilic attack by T12 onto γ -carbon of Asn



- Where does T12-OH proton go? Can substrate α -COO⁻ accept it?
- Is the acyl-enzyme intermediate stable?

Probing the reaction with QM

- Classical MD simulations not suitable to follow chemical rxns
- Use QM self-consistent field methods (Hartree-Fock, density functional theory)
 - Born-Oppenheimer approx. – separate wavefunction into nuclear and electronic components
 - Treat heavy nuclei as fixed point particles – focus on electrons
 - Iteratively solve time-independent Schrödinger eqtn. $H_{elec} \Psi_0 = E_{elec} \Psi_0$
 - *Ab initio* MD – classical trajectories of nuclei in quantum potential

$$\mathbf{F}_I = M_I \ddot{\mathbf{R}}_I = -\nabla_I V^{BO}(\mathbf{R}_I) = -\nabla_I \min_{\Psi_0} \left\{ \langle \Psi_0 | H_{elec} | \Psi_0 \rangle \right\}$$

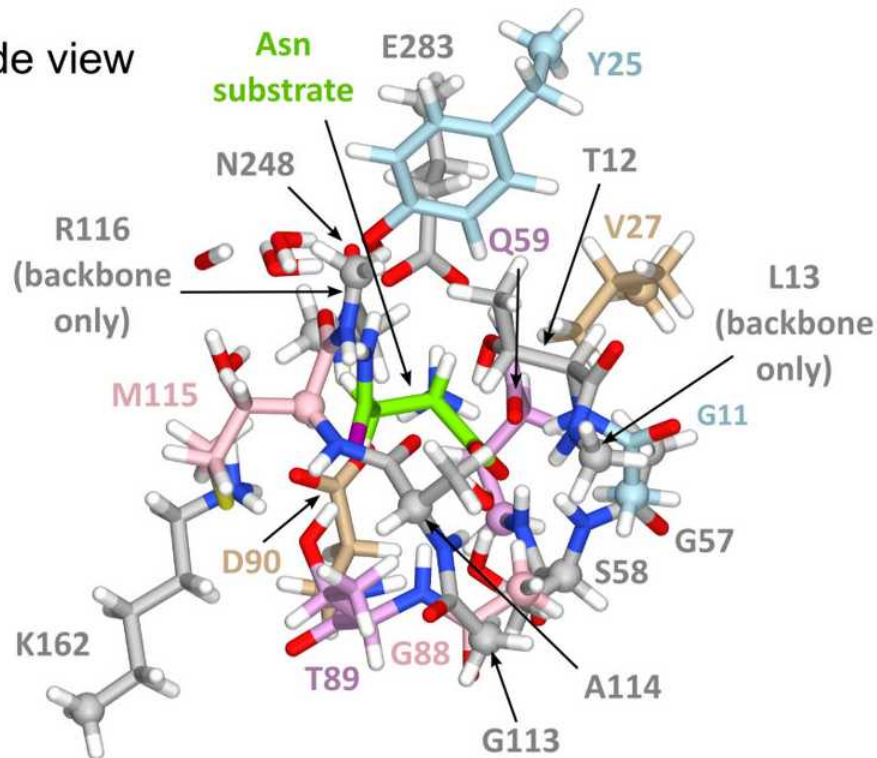
- Explore kinetics with *ab initio* MD based on regular MD results
- Calculate relative energies from stationary structures at various steps of reaction

Direct nucleophilic attack by T12

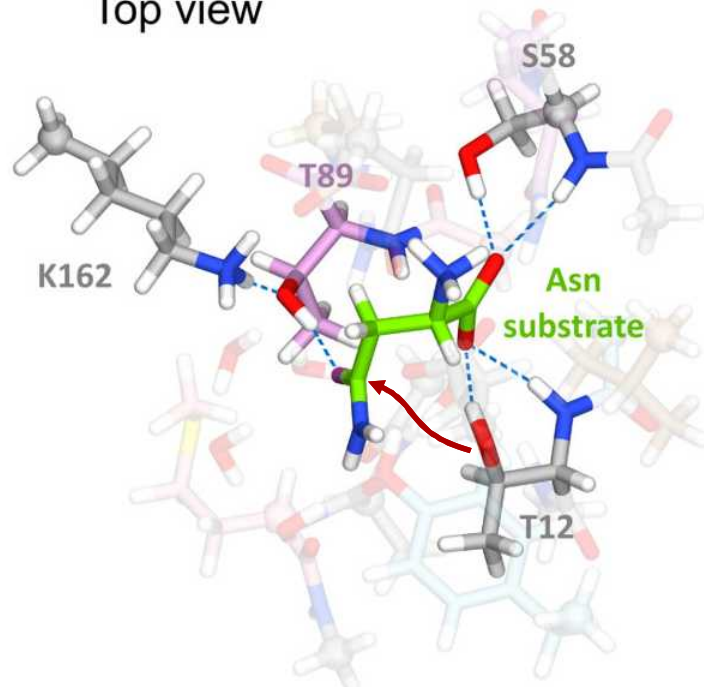
- QM system = active site amino acids + 4 waters – 239 atoms (α -carbons fixed)

- Starting configuration

Side view

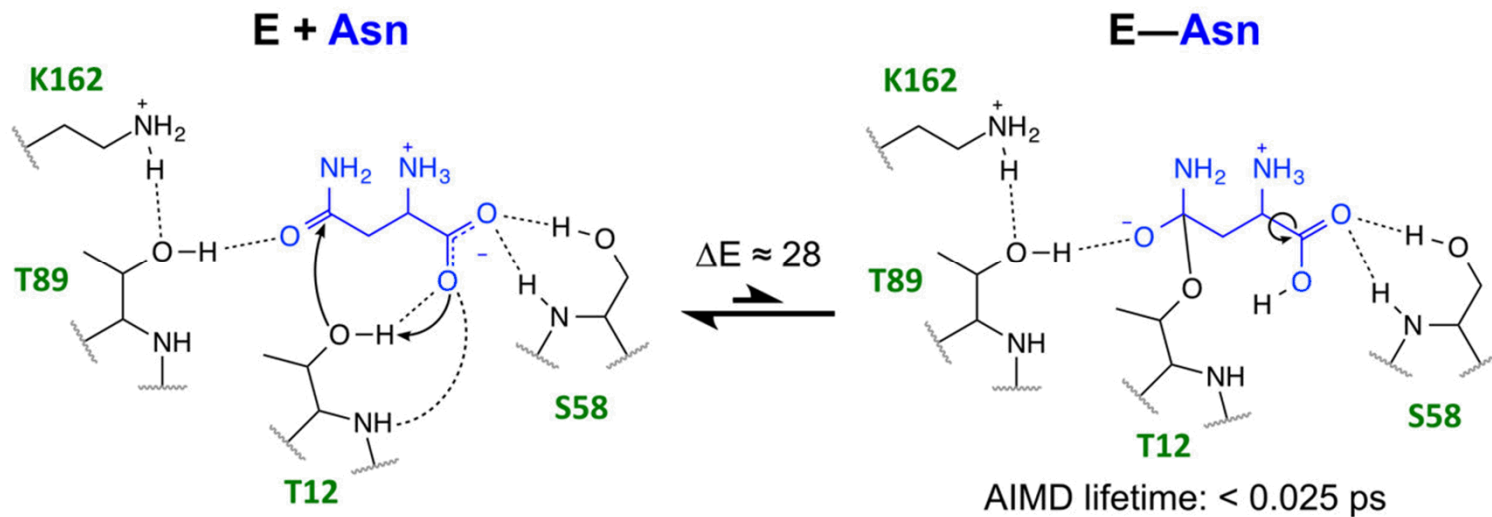
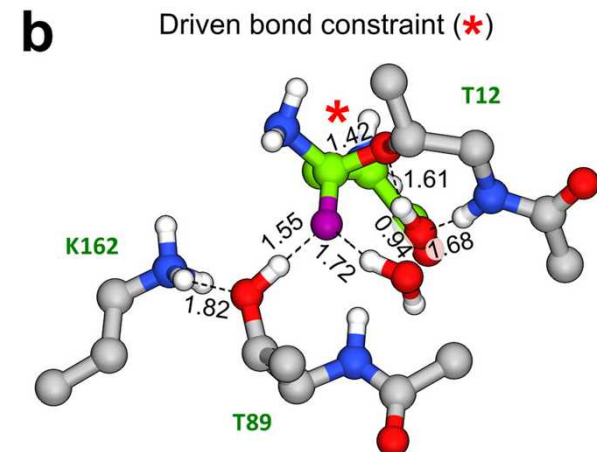


Top view



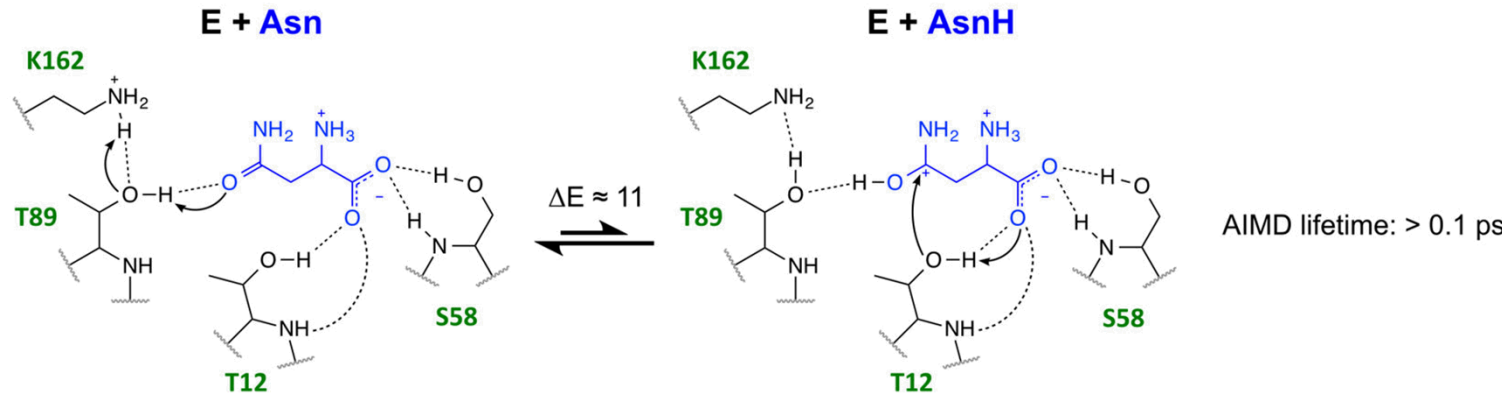
Direct nucleophilic attack by T12

- T12-OH proton spontaneously transfers to substrate α -COO⁻
- Enzyme-substrate covalent intermediate unstable (<0.025 ps)
- Relative energy of optimized end states \sim 28 kcal/mol



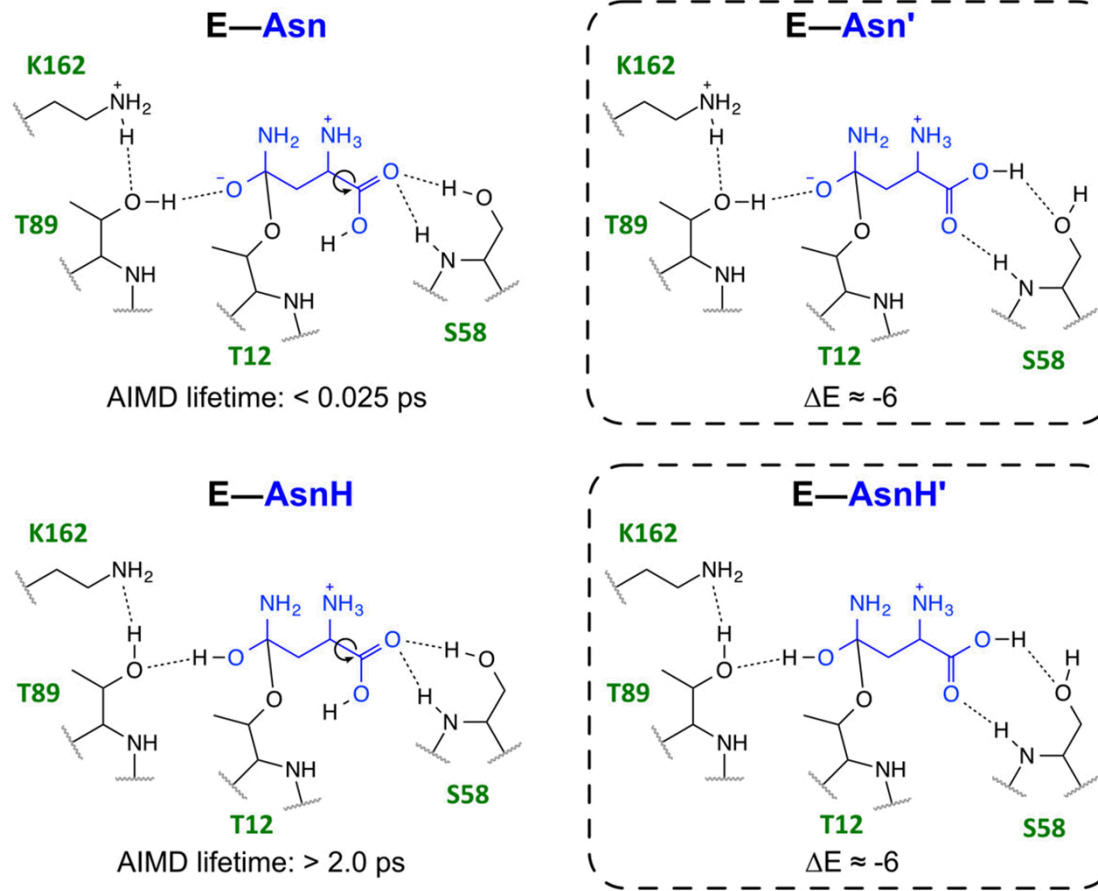
Pre-protonation stabilizes reaction

- Two-step attack by T12 is more kinetically favorable
 - Amide oxygen is first protonated by K162-T89 proton bridge



α -COOH prefers paired H-bonding

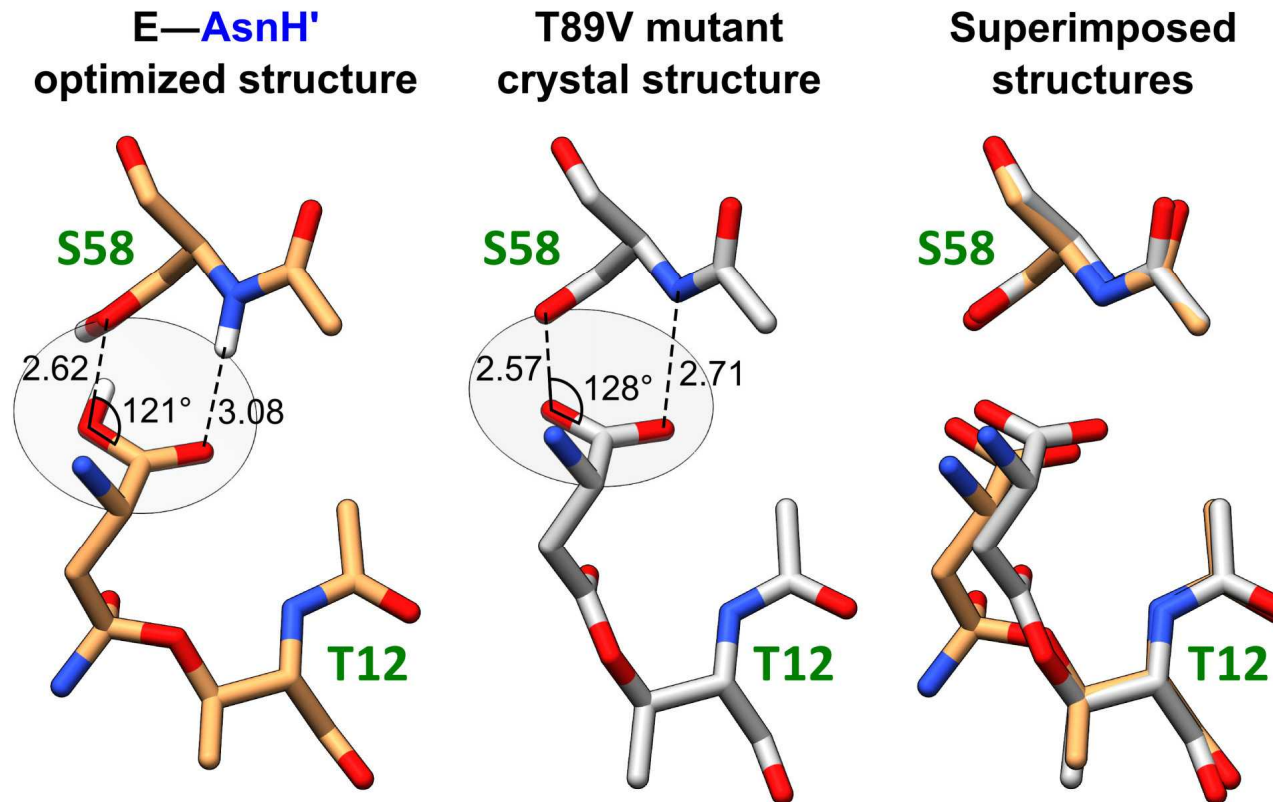
- Protonated α -COOH prefers a “paired” H-bonding pattern with S58 instead of being “clamped”



Anishkin, Vanegas et al. *J. Mol. Biol.* 427, 2867-2885 (2015)

QM structure similar to T89V mut.

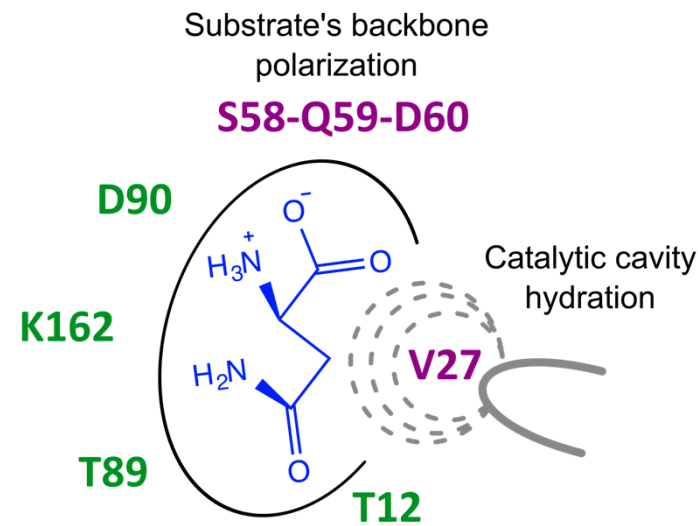
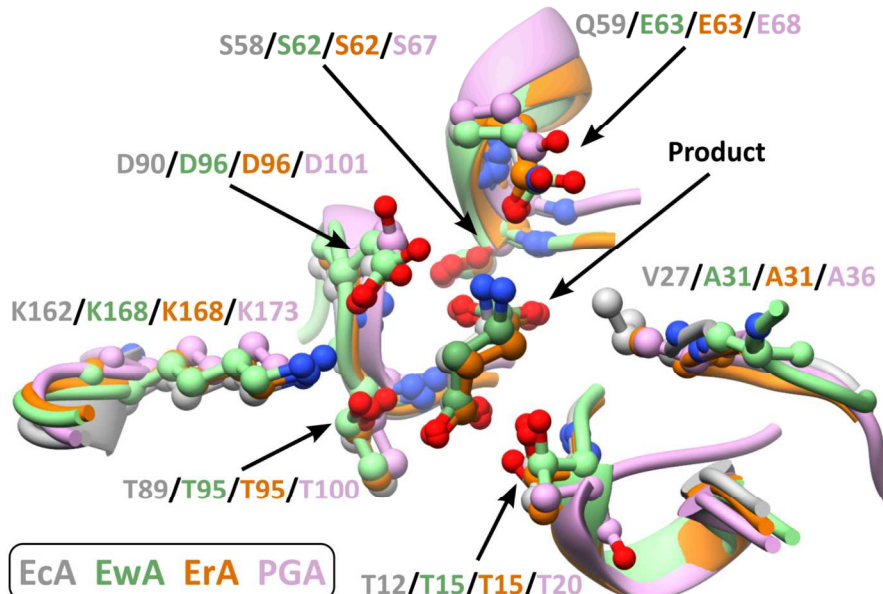
- E-AsnH' configuration similar to acyl-enzyme intermediate in T89V crystal structure (PDB 4ECA)
 - WT + mutant structures resemble intermediates, not initial state



Anishkin, Vanegas et al. *J. Mol. Biol.* 427, 2867-2885 (2015)

Ongoing work/future directions

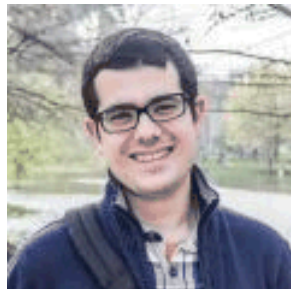
- Increasing catalytic rate of L-ASP requires knowledge of complete reaction mechanism
 - Mapping all reactions including energy barriers with QM/MM
- Comparison of *E. coli* L-ASP's structural features with enzymes from homologs (*Erwinia*, *Pseudomonas*, *Helicobacter*)



Acknowledgments



Dr. Marino Arroyo
UPC-BarcelonaTech



Alejandro Torres
UPC-BarcelonaTech



Dr. Susan Rempe
Sandia Natl. Labs



Dr. Philip Lorenzi
MD Anderson
Cancer Center (UT)



Dr. John Weinstein
MD Anderson
Cancer Center (UT)



Dr. Andriy Anishkin
U. of Maryland



Dr. Sergei Sukharev
U. of Maryland



European Research Council
Established by the European Commission



Barcelona
Supercomputing
Center
Centro Nacional de Supercomputación